24th COBEM - 2017

24th ABCM International Congress of Mechanical Engineering
December 3-8, 2017, Curitiba, PR, Brazil

COBEM-2017-1628
ROBUST CONTROL WITH VELOCITY FEEDBACK OF A CONTROL MOMENT GYROSCOPE

Bruno Augusto Angelico
Diego Colón
Escola Politécnica da Universidade de São Paulo, São Paulo, Brazil
angelico@lac.usp.br, diego@lac.usp.br

Abstract. *LQG/LTR is a robust control design technique based on frequency response, where the definition of stability and performance barriers plays a key role in its formulation. The stability robustness barrier depends on the inverse of the modeling error. For systems with pure resonance, the modeling error results in an infinite gain at the resonant frequency. This implies in an infinite attenuation at this frequency to the stability robustness barrier. This paper proposes a priori modification of the nominal model, so that the resonance peak is damped by a state feedback, eliminating the infinite attenuation in the stability robustness barrier. The methodology is applied to a Control Moment Gyroscope and practical results are presented in order to validate the proposed technique.*

Keywords: *Control Moment Gyroscope, Robust Control, Velocity Feedback, LQG/LTR*

1. INTRODUCTION

LQG/LTR is well established in Doyle and Stein (1981), Skogestad and Postlethwaite (2005) and Maciejowski (1989). It is well known that the linear quadratic regulator (LQR) presents good phase and gain margins, if all the states are perfectly measured and the weight matrix related to the control effort is diagonal. However, if the states have to be estimated by a Kalman filter, the resulting control strategy, also known as the Linear Gaussian Regulator (LQG), was shown to be *a priori* non-robust in Doyle (1978). In fact, there are no guarantees for the stability margins of the LQG controller. A method to design robust LQG controllers is the Loop Transfer Recovery (LTR) procedure, resulting in the LQG/LTR. The stability robustness barrier depends on the inverse of the modeling error. Such a barrier, which is a function of frequency, can be obtained by considering a percentage of error (e.g. $\pm 10\%$) in every model parameter and taking the singular value decomposition of the worst case error, considering all combinations. If the nominal model presents a pair of resonant poles, the barrier will have a singularity. A damping controller can be used prior to the LQG/LTR in order to handle such a problem.

Gyroscopic systems are nonlinear devices with a large spectrum of applications, as sensors and actuators. A Control Moment Gyroscope (CMG) is a special type of mechanic gyroscope mainly used for attitude control in spacecrafts and satellites (Bhat, 2006; Colón *et al.*, 2015a; Colón *et al.*, 2015b; Angelico *et al.*, 2015). It is also applied in the stabilization of unmanned vehicles (Yetkin *et al.*, 2014), anti-rolling and anti-pitching marine gyro-stabilizer system (Townsend and Shenoi, 2014), among others. A CMG consists in a spinning wheel (rotor) with motorized gimbals that changes the wheel's angular momentum, causing a gyroscopic torque that rotates a body in space. In general, they have torque motors that act in their axis to cause rotation in different direction (of the rotor) and then produce torque in the output axis. This process in general produces a torque amplification that must be sufficient to attitude control. The particular system that will be used in this work is from the ECP© manufacturer (Parks, 1999), which is represented in Fig. 1(a). A control design methodology is proposed consisting in a double loop control, in which the first (inner) loop has the objective of damping the nutation poles, and the second to provide robustness to the system.

In section 2, it is presented the LQG/LTR design methodology, in which is shown the importance of the stability and performance robustness barriers. In section 3, some steps in the process of obtaining the mathematical model of the CMG are presented, as well as the process of linearization for any arbitrary operation points. In section 4, the proposed double loop design process is presented for the ECP© didactic plant, with the experimental results presented in section 5. Finally, in section 6, the main conclusions are presented.

2. LQG/LTR ROBUST CONTROL BARRIERS

The nominal plant $G_N(s)$ has two inputs, toques T_3 and T_4, and two outputs, the angles θ_2 and θ_1 (position control). The controller $K(s)$ is also represented by a 2×2 transfer matrix, and the two outputs are used in the feedback. The

control system must obey the constraints of performance and stability that depends on an estimate error of the plant's model. Suppose that a standard linearized state space model of the system is provided, with constant matrices A, B, C and D. Assume that (A,B) is controllable and (C,A) is observable. Also, assume that there exists a superior limit $e_M(\omega)$ to the multiplicative error $\varepsilon_M(s) = [G_R(s) - G_N(s)]{G_N}^{-1}(s)$. In order to have stability robustness, the multivariable Nyquist criterion must be satisfied for all the candidate real plants $G_R(s)$, as shown in Athans (1986) and Stein and Athans (1987). It is supposed that all the possible real plants have the same number of unstable poles. The Nyquist criterion results in the following identity to be satisfied by the closed loop nominal system (the only that can be verified):

$$\frac{1}{e_M(\omega)} > \sigma_M[C_N(\omega)] \tag{1}$$

as $C_N(j\omega) = [I + G_N(j\omega)K(j\omega)]^{-1}G_N(j\omega)K(j\omega)$ and $\sigma_M(G)$ and $\sigma_m(G)$ stands for the maximum and minimum singular values of G, respectively. It is possible to simplify the expression to involve only the open loop transfer function matrix, but its validity is restricted to the frequency region that $e_M(\omega) >> 1$. The formula is simply $\frac{1}{e_M(\omega)} > \sigma_M[G_N(j\omega)K(j\omega)]$.

The performance requirements for the system must be specified in terms of the nominal system, and takes in consideration the error model $e_M(\omega)$. Those specifications must be in the frequency domain, using singular values of the transfer matrices, and must take in to account: 1) disturbance rejection, 2) insensitivity of the plant variations, 3) rejection of measurement error, and 4) reference tracking. If $e(j\omega)$ is the error (input to the controller), the following identities must be satisfied:

$$\frac{|e(j\omega)|}{|r(j\omega)|} \leq \alpha_r(\omega) << 1, \quad \frac{|e(j\omega)|}{|d(j\omega)|} \leq \alpha_d(\omega) << 1, \quad \frac{|y(j\omega)|}{|n(j\omega)|} \leq \alpha_n(\omega) << 1 \tag{2}$$

where $r(j\omega)$, $y(j\omega)$, $d(j\omega)$ and $n(j\omega)$ represent the frequency response of the reference, output, disturbance and measurement noise signal, respectively, while $\alpha_r(\omega)$, $\alpha_d(\omega)$ and $\alpha_n(\omega)$ are superior limits of the relations of the inequalities presented in Eq. (2).

If W_r is the frequency range of the reference signal, W_d is the frequency range of the disturbance signal and W_n is the frequency range of noise signal, it is possible to combine the first two barriers in a single one $p(\omega)$ that is the maximum of $\frac{1}{\alpha_r(\omega)}$, $\frac{1}{\alpha_d(\omega)}$, in each ω, and $W = W_r \cup W_d = \{\omega \in \mathbb{R} : \omega \leq \omega_0\}$ and $\omega_0 = \max\{\omega_r, \omega_d\}$. These barriers impose the following limits in the open loop singular values:

$$\sigma_m[G_N(j\omega)K(j\omega)] \geq p(\omega), \quad \sigma_M[G_N(j\omega)K(j\omega)] \leq \alpha_n(\omega) \tag{3}$$

The conditions above (nominal system) can be generalized to the specifications of the real system (for all class of plants). Considering modelling errors, such conditions can be written as:

$$\sigma_m[G_N(j\omega)K(j\omega)] \geq \frac{p(\omega)}{1-e_M(\omega)}, \quad \sigma_M[G_N(j\omega)K(j\omega)] \leq \frac{\alpha_n(\omega)}{1-e_M(\omega)} \tag{4}$$

3. MATHEMATICAL MODEL OF THE CONTROL MOMENT GYROSCOPE

The complete systems has four degrees of freedom, as shown in Fig. 1(b). The associated generalized coordinates are $\theta_1, \theta_2, \theta_3, \theta_4$ and are measured by corresponding encoders, from which it can be estimated the velocities $\dot{\theta}_1, \dot{\theta}_2, \dot{\theta}_3, \dot{\theta}_4$ by a first order backward approximation. Also, there are two DC motors (actuators), and the control inputs to the plant are: 1) the voltage applied to the DC motor 1 that runs the disc, generating torque T_4, and 2) the voltage applied to the DC motor 2, that runs the gimbal 3, generating T_3. The angular position of gimbal 2 (θ_2) is mainly controlled by the reaction torque produced by changing the speed of the wheel when the voltage of the DC motor 1 changes (T_4). On the other hand, the angular position of gimbal 1 (θ_1) is mainly controlled by changing the position of gimbal 3 when the voltage of the DC motor 2 changes (T_3) (gyroscope precession).

The nonlinear dynamic equations are obtained by the Lagrange method, where L is the Lagrangian, T_n is the torque in axis n, $\dot{\theta}_n = \omega_n$ and $n = 1,2,3,4$. As all the centers of mass of all the bodies (rotor and gimbals) are located in the center of mass of the rotor, as well as the origin of the inertial reference frame $\{0\}$, the system's Lagrangian function is only the kinetic energy, that is given by:

$$L = \sum_{n=1}^{4} \left[\frac{1}{2} \cdot m_n \cdot V_{c_n}^{\top} \cdot V_{c_n} + \frac{1}{2} \cdot {}^{n}\Omega_n{}^{\top} \cdot (I_n \cdot {}^{n}\Omega_n) \right] \tag{5}$$

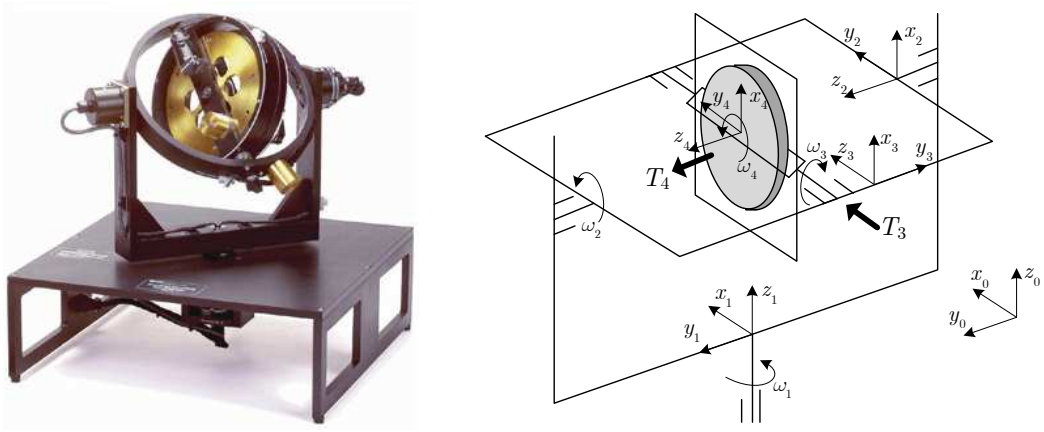

(a) (b)

Figure 1. Control Moment Gyroscope System: a) photo of ECP© system (Parks, 1999), b) Gyroscope scheme.

where n represents the n-th rigid body ($n = 1$ is the outer gimbal and $n = 4$ is the flywheel), m_n is the mass of the rigid body n, V_{c_n} is the velocity of the center of mass of the rigid body n in the inertial system $\{0\}$, ${}^n\Omega_n$ is the angular velocity vector of the rigid body n in the reference frame $\{n\}$, I_n is the inertia tensor of the rigid body n. The CMG's rigid bodies do not translate, that is $V_{c_n} = 0$. After some manipulation, the resulting Lagrangian is:

$$\begin{aligned} L \;=\; & \tfrac{I_c\,\omega_3^2}{2} + \tfrac{I_d\,\omega_3^2}{2} + \tfrac{J_b\,\omega_2^2}{2} + \tfrac{J_d\,\omega_4^2}{2} + \tfrac{K_a\,\omega_1^2}{2} + \tfrac{J_c\,\omega_2^2\cos^2\theta_3}{2} + \tfrac{J_d\,\omega_2^2\cos^2\theta_3}{2} + \\ & \tfrac{K_b\cos^2\theta_2}{2} + \tfrac{I_b\,\omega_1^2\sin^2\theta_2}{2} + \tfrac{I_c\,\omega_1^2\sin^2\theta_2}{2} + \tfrac{I_d\,\omega_1^2\sin^2\theta_2}{2} + \\ & \tfrac{I_d\,\omega_2^2\sin^2\theta_3}{2} + \tfrac{K_c\,\omega_2^2\sin^2\theta_3}{2} + \tfrac{I_d\,\omega_1^2\cos^2\theta_2\cos^2\theta_3}{2} + \\ & \tfrac{K_c\,\omega_1^2\cos^2\theta_2\cos^2\theta_3}{2} + \tfrac{J_c\,\omega_1^2\cos^2\theta_2\sin^2\theta_3}{2} + \tfrac{J_d\,\omega_1^2\cos^2\theta_2\sin^2\theta_3}{2} + \\ & J_d\,\omega_4\omega_2\cos\theta_3 - I_c\,\omega_1\,\omega_3\sin\theta_2 - I_d\,\omega_1\,\omega_3\sin\theta_2 + J_d\,\omega_4\,\omega_1\cos\theta_2\sin\theta_3 - \\ & I_d\,\omega_2\,\omega_1\cos\theta_2\cos\theta_3\sin\theta_3 + J_c\,\omega_1\,\omega_2\cos\theta_2\cos\theta_3\sin\theta_3 + \\ & J_d\,\omega_1\,\omega_2\cos\theta_2\cos\theta_3\sin\theta_3 - K_c\,\omega_1\,\omega_2\cos\theta_2\cos\theta_3\sin\theta_3 \end{aligned} \tag{6}$$

The non-linear model was linearized around the following equilibrium point: $\theta_1 = 0$, $\theta_2 = -20^\circ$, $\theta_3 = 20^\circ$, $\omega_1 = \omega_2 = \omega_3 = 0$, and $\omega_4 = \Omega = 400$ rpm. After linearizing and using θ_i instead of $\Delta\theta_i$ for the small variations, the complete model has the following states: $\theta_1, \theta_2, \theta_3$ and $\omega_1, \omega_2, \omega_3, \omega_4$, so the system has order seven. The angular velocity ω_4 is considered constant, and its corresponding equation can be eliminated. Moreover, the equation regarding θ_3 is also eliminated, since it does not affect the controlled angles θ_1 and θ_2. Its angular velocity, ω_3 does affect θ_1 and θ_2 and cannot be eliminated. The resulting system is controllable, observable and with a minimum phase transmission zeros, and its state, input and output vectors are : $\mathbf{x} = [\theta_2\ \theta_1\ \omega_3\ \omega_2\ \omega_1]^\top$, $\mathbf{u} = [T_4\ T_3]^\top$, $\mathbf{y} = [\theta_2\ \theta_1]^\top$.

The inertial parameters are given by Parks (1999): $I_B = 0.0119$, $I_C = 0.0124$, $I_D = 0.0148$, $J_B = 0.0178$, $J_C = 0.0281$, $J_D = 0.0273$, $K_A = 0.0693$, $K_B = 0.0297$ and $K_C = 0.0188$ ($Kg \cdot m^2$). With these values, it is possible to obtain a linearized model in S.I. unities. Considering the control efforts gains $k_{u_1} = 2.1544 \times 10^{-5}$ and $k_{u_2} = 8.9355 \times 10^{-5}$ ($N \cdot m/counts$), and the encoders gains $k_{e_1} = k_{e_2} = 81504$, $k_{e_3} = 124256$ and $k_{e_4} = 33952$ ($counts/rad$), the model is expressed in unities of encoder pulses and digital to analog converter (DAC) counts, which is more suitable for control design. A state space representation is obtained, with:

$$A = \begin{bmatrix} 0 & 0 & 0 & 1 & 0 \\ 0 & 0 & 0 & 0 & 1 \\ 0 & 0 & 2.7039 & -21.9216 & 58.0068 \\ 0 & 0 & 5.3269 & 0 & 2.7776 \\ 0 & 0 & -5.1857 & & -2.7039 \end{bmatrix}, \quad B = \begin{bmatrix} 0 & 0 \\ 0 & 0 \\ 2.5799 & 418.5058 \\ -35.6280 & -0.7057 \\ -4.9478 & -19.7750 \end{bmatrix}, \tag{7}$$

4. CONTROL DESIGN

The major drawback in the application of LQG/LTR methodology in systems with pure imaginary poles is that the modeling error, $e_M(\omega)$, will have a resonance peak that is infinity in some frequency. Due to the fact that the performance and stability barriers depend on the inverse of $e_M(\omega)$, the process of adjusting the singular values between the barriers cannot be properly done, as shown in Fig. 2 (continuous line). In this case, the modeling error was assumed as $\pm 10\%$ variation in all inertial parameters and in the wheel velocity.

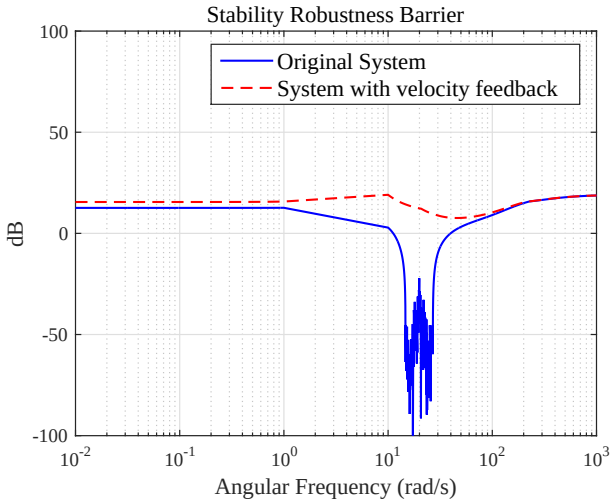

Figure 2. Stability robustness barriers with and without velocity feedback.

4.1 Velocity State Feedback and the Redefinition of the Stability Robustness Barrier

A very well-known method to introduce damping in mechanical systems is by velocity feedback (Dorf and Bishop, 2010). It will be shown that by using the angular velocity states of the CMG as feedback variables, one can displace the pure imaginary poles to the open left complex plane. The higher noise level from the discrete differentiation of the encoder (velocity calculation) is not a problem thanks also to the velocity feedback. It is easy to see that the CMG model in section 3 has the form (in which the sub-matrices A_{11} and A_{21} are always zero):

$$A = \left[\begin{array}{cc|ccc} 0 & 0 & 0 & 1 & 0 \\ 0 & 0 & 0 & 0 & 1 \\ \hline 0 & 0 & A_{22}^1 & A_{22}^2 & A_{22}^3 \\ 0 & 0 & A_{22}^4 & 0 & A_{22}^5 \\ 0 & 0 & A_{22}^6 & 0 & A_{22}^7 \end{array}\right] = \left[\begin{array}{c|c} A_{11} & A_{12} \\ \hline A_{21} & A_{22} \end{array}\right] \quad B = \left[\begin{array}{cc} 0 & 0 \\ 0 & 0 \\ \hline B_2^1 & B_2^2 \\ B_2^3 & B_2^4 \\ B_2^5 & B_2^6 \end{array}\right] = \left[\begin{array}{c} B_1 \\ \hline B_2 \end{array}\right] \tag{8}$$

As $\det(A) = \det(A_{11})\det(A_{22} - A_{21}A_{11}^{-1}A_{12})$ (Zhou *et al.*, 1996), it can be observed that Eq. (8) has the spectrum equal to the eigenvalues of A_{11} and A_{22}. This means that the eigenvalues are $\{0, 0\}$ and three other values depending on A_{22}. From Eq. (7), these values are $\{0, j19.9758, -j19.9758\}$. The velocity state feedback has structure as presented in Eq. (9), and only affects the poles of the sub-matrix A_{22}, as $(A - BK)$ has the same structure of Eq. (8). Also, as the reduced characteristic equation has order three, it is only necessary three non-zero feedback gains. One reasonable choice consists in feeding back ω_1 in θ_1, ω_2 in θ_2, and ω_3 in θ_1. The last is due to the coupling between the velocity of gimbal #3 and the position of gimbal #1. Hence:

$$K = \left[\begin{array}{cc|ccc} 0 & 0 & 0 & K_1 & 0 \\ 0 & 0 & K_2 & 0 & K_3 \end{array}\right] = [0 \,|\, K_r] \tag{9}$$

The closed loop state matrix, considering the sub-matrices A_{22} and B_2, and the feedback matrix K_r is given by:

$$A_c = (A_{22} - B_2 \cdot K_r) = \left[\begin{array}{ccc} A_{22}^1 - B_2^2 K_2 & A_{22}^2 - B_2^1 K_1 & A_{22}^3 - B_2^2 K_3 \\ A_{22}^4 - B_2^4 K_2 & -B_2^3 K_1 & A_{22}^5 - B_2^4 K_3 \\ A_{22}^6 - B_2^6 K_2 & -B_2^5 K_1 & A_{22}^7 - B_2^6 K_3 \end{array}\right] \tag{10}$$

Its desired to allocate the closed loop poles at $p = [-31.5592 \;\; -15.5834 \;\; -2.2250]$. Hence the characteristic equation is given by $s^3 + 49.3676s^2 + 596.6919s + 1094.3 = 0$. On the other hand, from Eq. (10), and substituting the coefficients of A_{22} and B_2, it follows that:

$$\begin{aligned} &s^3 + (465.42K_2 - 34.923K_1 - 21.577K_3)s^2 + (747.39K_1K_3 - 5.7657 \times 10^{-14}K_2 - 2.2907 \times 10^3 K_3 \\ &- 1.6251 \times 10^4 K_1K_2 - 4.7166 \times 10^{-15}K_1 + 399.0310)s - (1.1448 \times 10^4 K_1 - 1.3483 \times 10^3 K_2 \\ &+ 2.5858 \times 10^3 K_3 + 5.6036 \times 10^3 K_1K_2 - 9.1870 \times 10^4 K_1K_3 + 9.3711 \times 10^{-14}) = 0 \end{aligned} \tag{11}$$

Comparing the characteristic equation and Eq. (11), it results in a system with three non-linear algebraic equations. By using the MATLAB Symbolic Math Toolbox, the system is solved, resulting in three different set of solutions:

$$K_r' = \begin{bmatrix} 0 & -0.2832 & 0 \\ 0.0887 & 0 & 0.0842 \end{bmatrix}, \; K_r'' = \begin{bmatrix} 0 & -1.0621 & 0 \\ 0.0316 & 0 & 0.1128 \end{bmatrix}, \; K_r''' = \begin{bmatrix} 0 & -0.05 & 0 \\ 0.1 & 0 & -0.05 \end{bmatrix} \quad (12)$$

For the sake of numerical simplicity, the rightmost solution in Eq. (12) is adopted. The new stability robustness barrier is also shown in Fig. 2 (dashed red line). As can be seen, the singularity does not exist anymore. In Figure 3 it is presented the pole-zero map with and without velocity feedback, considering $\pm 10\%$ variation in the inertial parameters and in the wheel velocity. The poles of the modified system do not reach the imaginary axis, which means that there are no resonant poles for a candidate real system.

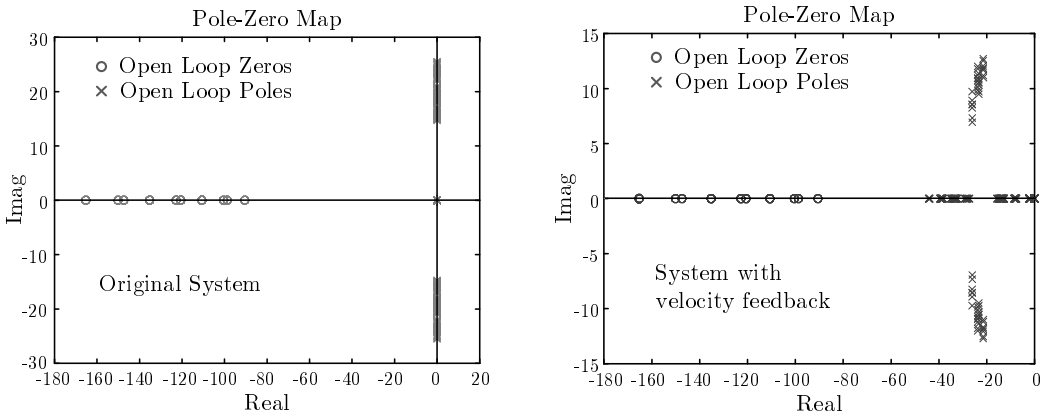

(a) (b)

Figure 3. Pole-zero map with 10% variation in the model parameters: (a) original system; (b) system with velocity feedback.

4.2 LQG/LTR Design

The frequency response of the modeling error, $e_M(\omega)$, is obtained considering 10% of uncertainty in all parameters, and the stability robustness barrier is considered as being the worst case possible in each ω. It is also assumed that the low frequency barrier must reject 10% of disturbance and 5% of signal following reference error. The high frequency barrier must reject 90% of the measurement noise. The objective open loop is presented in Fig. 4, where it is possible to see that the singular values fit properly between the barriers, guaranteeing the specifications. The robustness stability barrier, $1/e_M(\omega)$ in decibels, is shown in red line, while the barriers of low and high robustness performance (disturbance and noise rejection, respectively) are shown in gray. In order to obtain this situation, the parameters μ and L had to be carefully chosen, and one integrator was introduced in each channel, in order to eliminate a stationary error due to the Coulomb friction, resulting two additional states. In Figure 5(a) it is possible to see the recovered open loop singular values for $\rho = 10^{-4}$, which also fit the barriers, while Fig. 5(b) presents the closed loop singular values (recovered), which guarantees that the robust stability condition is satisfied.

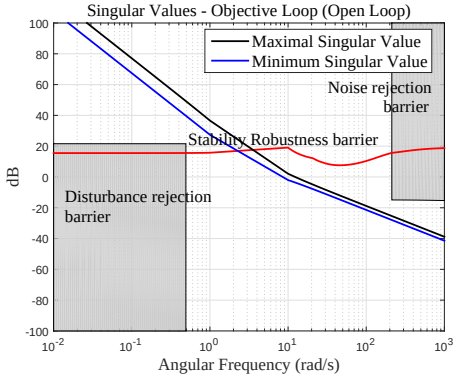

Figure 4. Objective Open Loop.

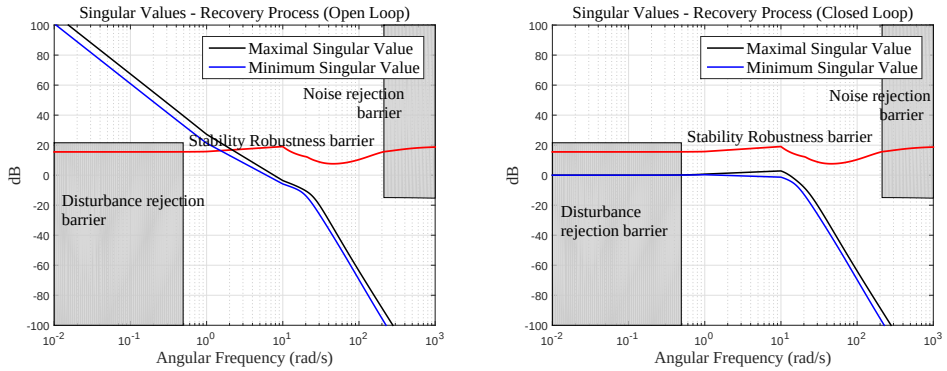

(a) Recovered Open Loop. (b) Recovered Closed Loop

Figure 5. Recovered Singular values.

5. EXPERIMENTAL RESULTS

In this section, it is presented the experimental results obtained in the ECP© CMG. The experimental setup is shown in Fig. 6. The control algorithm is implemented in MATLAB/Simulink and compiled with Real Time Windows Target. The personal computer has a PCI target connected to the I/O electronics unit by a flat cable. This unit has a power amplifier, the break manual switches and makes the interconnections between the PC and the mechanical system.

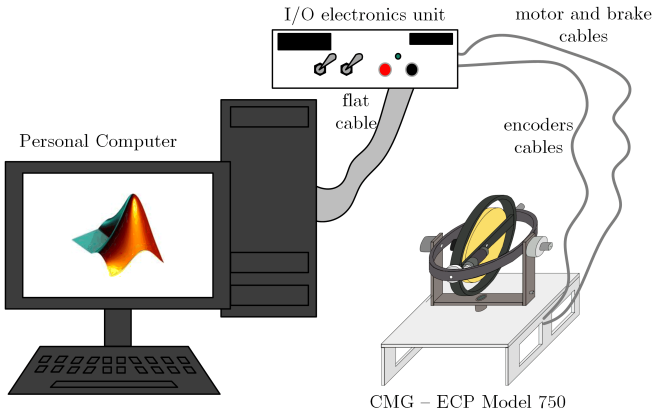

Figure 6. Experimental setup.

Before the multivariable control starts, the system is taken to its operation point. Gimbal #2 and #3 angles are positioned such that $\theta_2 = -20^\circ$ and $\theta_3 = 20^\circ$, and brakes of axes 1 and 2 are turned on. Hence, an initial control loop with a simple PI speed controller acts in motor M#1 in order to speed the rotor disk (flywheel) to 400 rpm. About 13 seconds later, breaks are manually released, since the system is in equilibrium. At 15 seconds, the multivariable control algorithm starts and the velocity control stops.

Figure 7 and Figure 8 present the control tracking performance. In the first, a step of 10° is applied to the θ_1 reference in 25 seconds, and the same step is applied to θ_2 in 35 seconds. This procedure is repeated for a step variation of -10°, as shown in Fig. 8. Figure 7 (b) and Figure 8 (b) brings the flywheel speed variations during the experiments. The control signals are presented in Fig. 7 (c, d) and Fig. 8 (c, d). As can be seen in both cases, the system is able to track the reference with good performance, the flywheel speed remain around the 400 RPM and the control efforts for both M#1 and M#2 are well limited after the multivarible control starts.

Figure 9 and Figure 10 show the disturbance rejection experiments in regulatory mode. The same procedure described for the control tracking performance is conducted to lead the system to its operation point. In Figure 9 (a), a positive rectangular pulse disturbance of 10 seconds duration is applied at the plant's input at 25 seconds for θ_2 channel, and at 35 seconds for θ_1 channel. The same is done for the results of Fig. 10 (a), but with a negative rectangular pulse. The control signals are shown in Fig. 9 (c, d) and Fig. 10 (c, d), respectively. In both cases, the control algorithm is able to reject the disturbance and the control signals are well behaved. It is also noted that in the latter case, the wheel speed left the linear region, but the control still had a good performance.

Next results take into account the sinusoidal tracking and disturbance rejection. In Fig. 11 it was assumed a sine input with amplitude 5° and frequency 0.4 rad/s in both channels with $\pi/2$ phase shift. As can bee seen, the system was able to

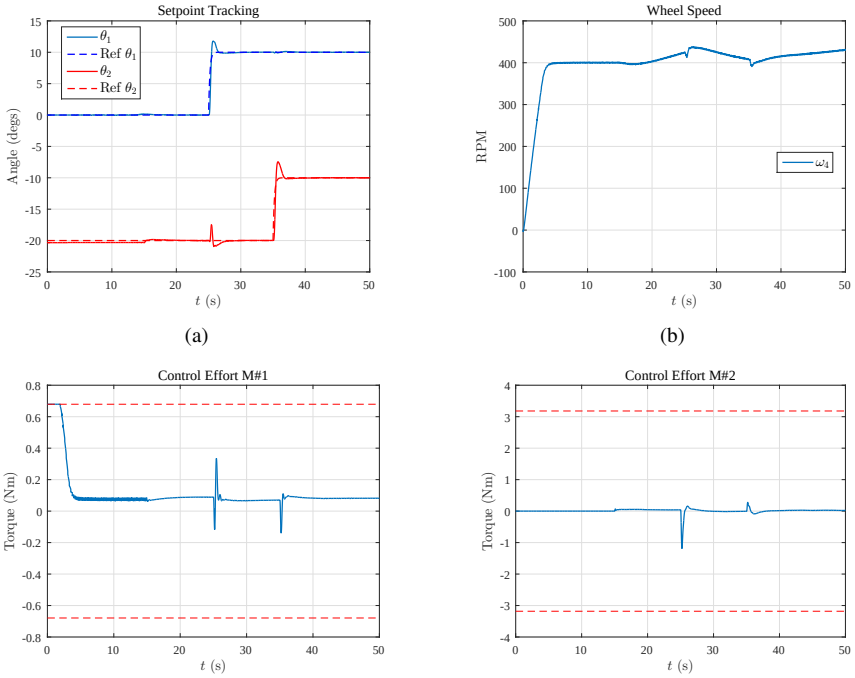

Figure 7. Results for positive step response of +10° for both θ_1 and θ_2: a) step response, b) wheel speed, c) control effort applied to M1, d) control effort applied to M#2.

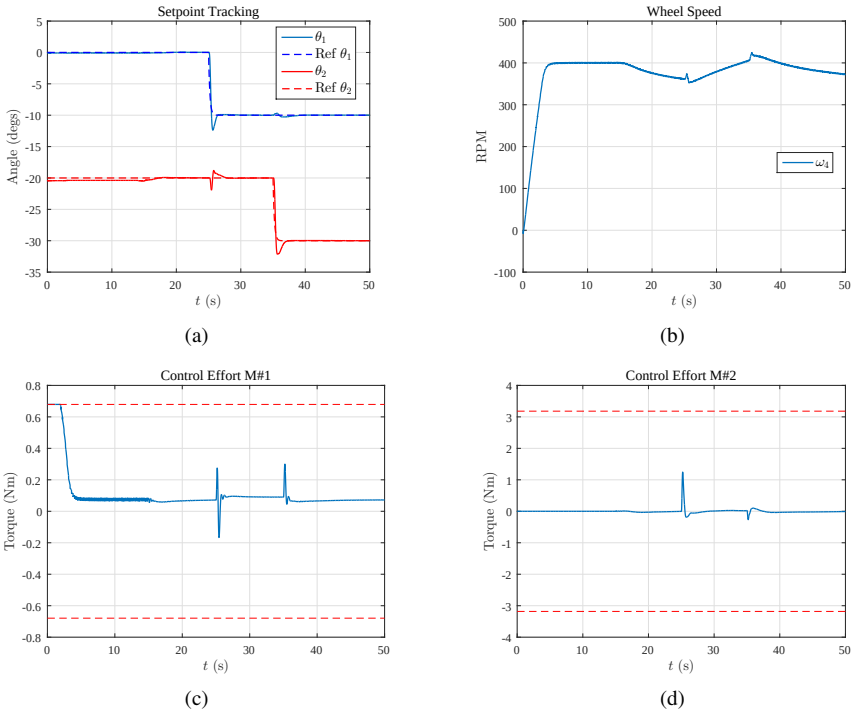

Figure 8. Results for negative step response of -10° for both θ_1 and θ_2: a) step response, b) wheel speed, c) control effort applied to M#1, d) control effort applied to M#2.

track the reference in steady state according to the design specification.

Figure 12 shows the results for a sinusoidal disturbance at the plant's output. A sine signal with amplitude 5° and frequency 0.4 rad/s was added in both channels with $\pi/2$ phase shift. The system could reject this disturbance according to the design specifications.

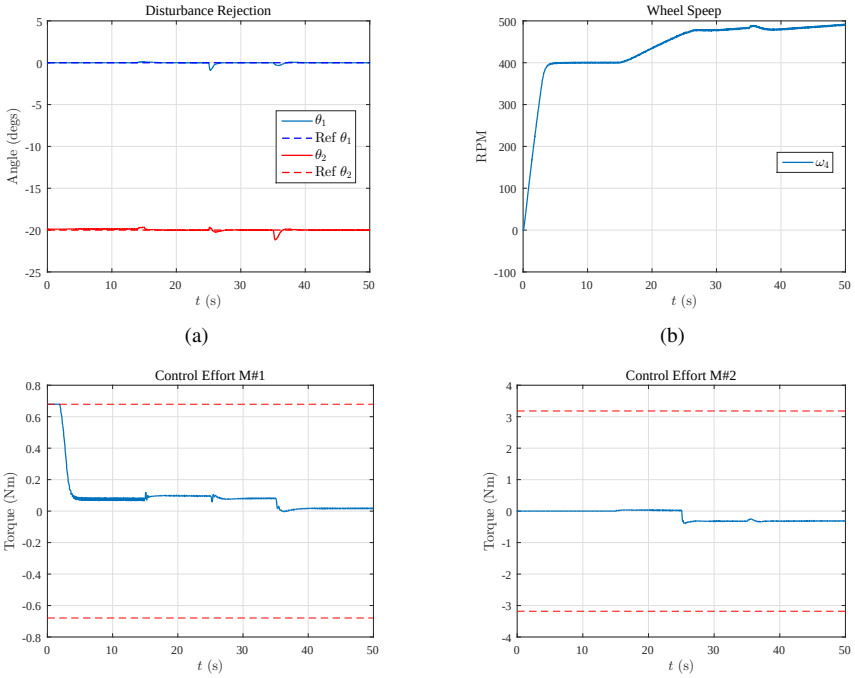

Figure 9. Results for positive step disturbance for both θ_1 and θ_2: a) step response, b) wheel speed, c) control effort applied to M#1, d) control effort applied to M#2.

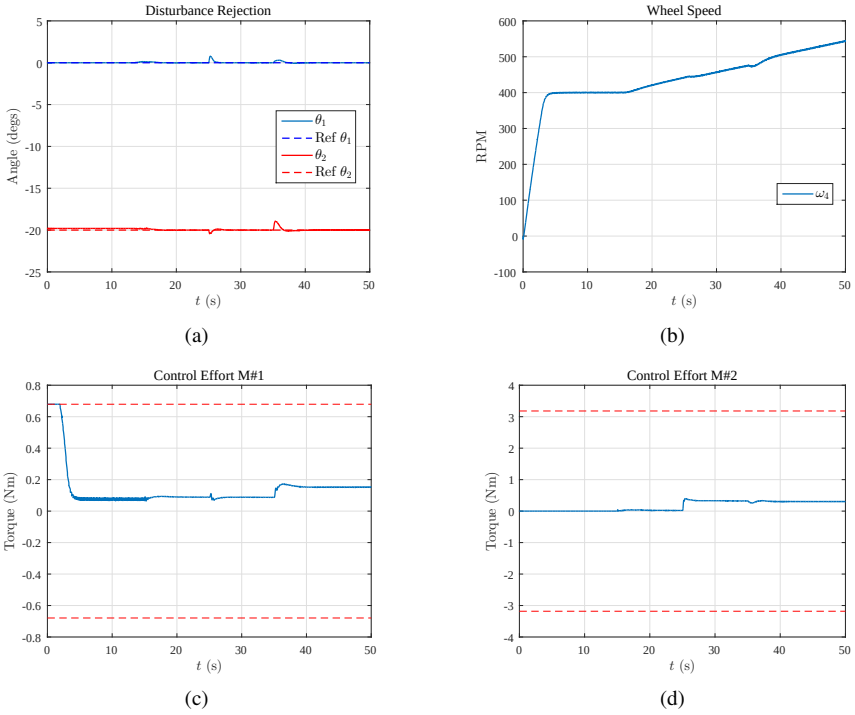

Figure 10. Results for negative step disturbance for both θ_1 and θ_2: a) step response, b) wheel speed, c) control effort applied to M#1, d) control effort applied to M#2.

6. CONCLUSIONS

It is presented a method to design a LQG/LTR robust controller for a system with poles in the imaginary axis. These poles directly influence the robust stability barrier. An inner loop was designed by directly allocating the closed-loop poles in a position with damping, which eliminates the stability barrier problem. It consisted in a velocity feedback that guaranteed the system damping and a reduced feedback noise. After that, a second loop, that gives robustness to the system, was designed. Practical results were presented in order to validate the proposed method.

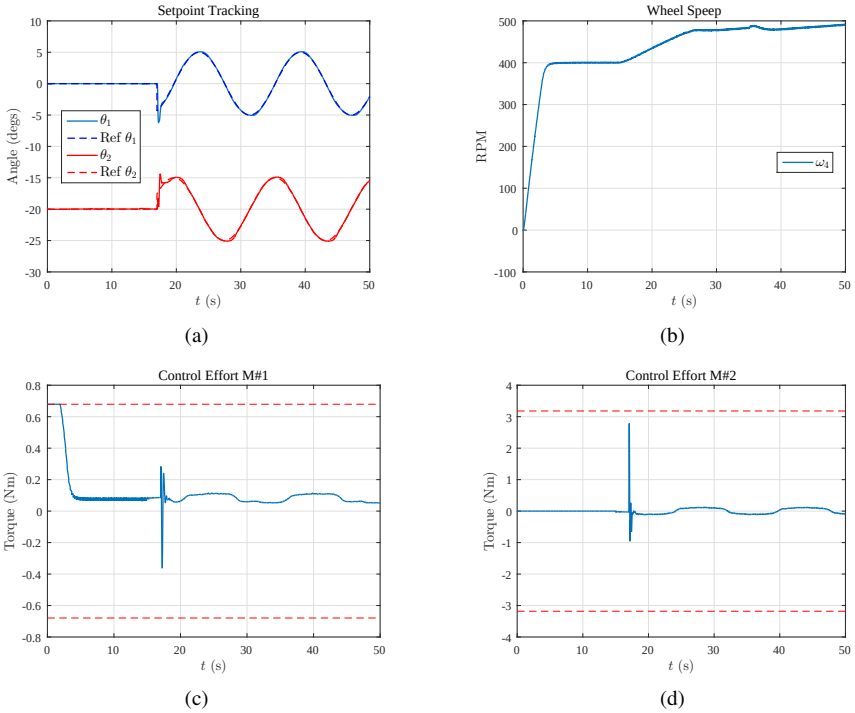

Figure 11. Results for sinusoidal set-point tracking for both θ_1 and θ_2: a) step response, b) wheel speed, c) control effort applied to M#1, d) control effort applied to M#2.

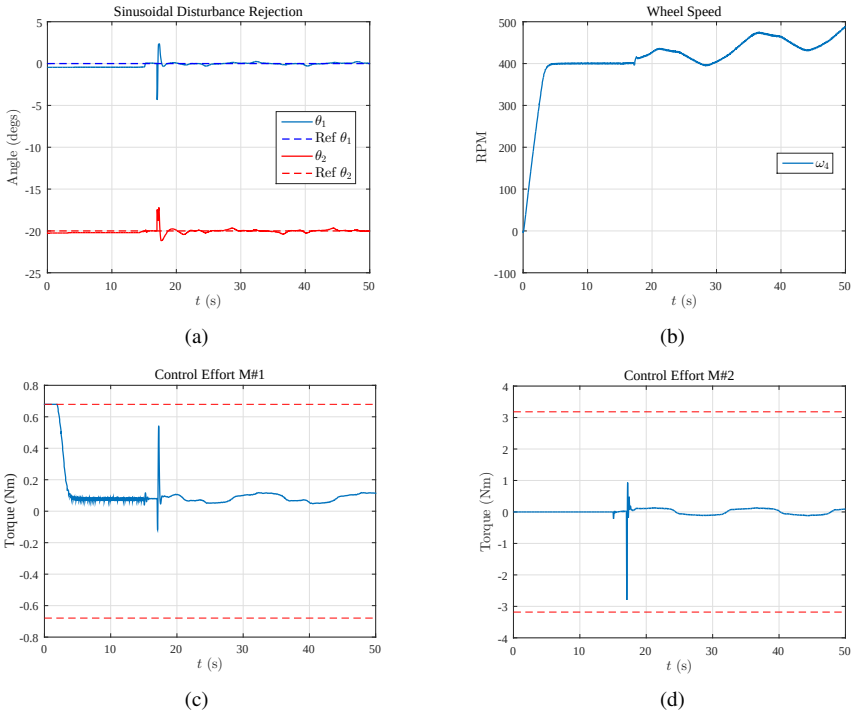

Figure 12. Results for negative step disturbance for both θ_1 and θ_2: a) step response, b) wheel speed, c) control effort applied to M#1, d) control effort applied to M#2.

7. ACKNOWLEDGEMENTS

The authors would like to thank Fundação de Amparo à Pesquisa do Estado de São Paulo (FAPESP) for the grant 2013/25605-2.

8. REFERENCES

Angelico, B.A., Colón, D. and Balthazar, J.M., 2015. "Modeling and h infinity control of a control moment gyroscope". In *Proceedings of the 23rd ABCM International Congress of Mechanical Engineering*. ABCM.

Athans, M., 1986. "A tutorial on the LQG/LTR method". In *American Control Conference, 1986*. pp. 1289–1296.

Bhat, S., 2006. "Controllability of spacecraft attitude using control moment gyroscopes". In *American Control Conference (ACC)*. pp. 5 pp.–.

Colón, D., Angélico, B.A. and Balthazar, J.M., 2015a. "Robust control of a variable speed control moment gyroscope". *Mathematics in Engineering, Science and Aerospace (MESA)*, Vol. 6, No. 3, pp. 453–474.

Colón, D., Angelico, B.A., Toriumi, F.Y., Liduário, P.U.M. and Balthazar, J.M., 2015b. "Geometric modeling and robust control of a gyroscopic system". In *Proceedings of the ASME 2015 IDETC/CIE 2015*. ASME, Boston, Vol. 8.

Dorf, R. and Bishop, R., 2010. *Modern Control Systems*. Pearson Prentice Hall, 12th edition.

Doyle, J. and Stein, G., 1981. "Multivariable feedback design: Concepts for a classical/modern synthesis". *IEEE Transactions on Automatic Control*, Vol. 26, No. 1, pp. 4–16.

Doyle, J., 1978. "Guaranteed margins for LQG regulators". *IEEE Transactions on Automatic Control*, Vol. 23, No. 4, pp. 756–757.

Maciejowski, J.M., 1989. *Multivariable feedback design*. Electronic systems engineering series. Wokingham, England Reading, Mass. Addison-Wesley.

Parks, T.R., 1999. *Manual For Model 750 Control Moment Gyroscope*. ECP - Educational Control Products, California, USA, 1st edition.

Skogestad, S. and Postlethwaite, I., 2005. *Multivariable Feedback Control: Analysis and Design*. John Wiley & Sons. ISBN 0470011688.

Stein, G. and Athans, M., 1987. "The LQG/LTR procedure for multivariable feedback control design". *IEEE Transactions on Automatic Control*, Vol. 32, No. 2, pp. 105–114.

Townsend, N. and Shenoi, R., 2014. "Control strategies for marine gyrostabilizers". *IEEE Journal of Oceanic Engineering*, Vol. 39, No. 2, pp. 243–255.

Yetkin, H., Kalouche, S., Vernier, M., Colvin, G., Redmill, K. and Ozguner, U., 2014. "Gyroscopic stabilization of an unmanned bicycle". In *American Control Conference (ACC)*. pp. 4549–4554.

Zhou, K., Doyle, J.C. and Glover, K., 1996. *Robust and Optimal Control*. Prentice-Hall, Inc., Upper Saddle River, NJ, USA.

9. RESPONSIBILITY NOTICE

The authors are the only responsible for the printed material included in this paper.